JOURNAL OF PROPULSION AND POWER
Vol. 25, No. 1, January–February 2009

Experimental Investigation of an Embedded Crossflow Fan for Airfoil Propulsion/Circulation Control

Ryan K. Dygert* and Thong Q. Dang†
Syracuse University, Syracuse, New York 13244

DOI: 10.2514/1.37110

This experimental study examines the feasibility and effectiveness of using a crossflow fan embedded in an airfoil for simultaneous propulsion and circulation control. In an earlier computational fluid dynamics study, results indicated that a 34% thick airfoil equipped with a trailing-edge-embedded crossflow fan can operate stall-free up to 40 deg angle of attack and achieve lift coefficients upward of 6–7. This study seeks to experimentally verify the computational fluid dynamics results and provide further insight into the fan's behavior in providing circulation control to the airfoil. Through flow-visualization techniques, surface static pressure, and wake total pressure measurements, the degree to which the fan can influence the flow is determined. Surface pressure distributions are studied for a wide range of fan operating points and angles of attack, leading ultimately to the calculation of the relative improvement in the airfoil's lift-coefficient curves for the cases studied. Finally, the experimental setup and geometry were reproduced in the computational fluid dynamics package FLUENT for direct comparison with the acquired data. Good agreement between the experimental data and computational fluid dynamics results was found and both confirm the viability of the proposed propulsive/circulation-control airfoil concept.

Nomenclature

Cp	=	static pressure coefficient, $(p - p_s)/(U^2/2)$
C^*p_o	=	wake/jet region corrected total pressure coefficient, $\{(p_0 - \rho V_y^2/2) - p_{\text{atm}}\}/(\rho U^2/2)$
C_l	=	lift coefficient, $L/(\rho U^2 c/2))$
c	=	airfoil chord
c_b	=	fan blade chord
D	=	fan diameter
l	=	lift per unit span
N	=	fan rotational speed
p	=	surface static pressure
p_{atm}	=	freestream total pressure
p_s	=	tunnel static pressure, $\{p_{\text{atm}} - U^2/2\}$
p_0	=	total pressure
Re_c	=	Reynolds number based on airfoil chord, $\rho U c/\mu$
Re_f	=	Reynolds number based on the fan, $\rho U c_b/\mu$
t	=	airfoil maximum thickness
U	=	freestream velocity
u	=	blade tip speed
V_y	=	jet vertical-velocity component
α	=	angle of attack
μ	=	dynamic viscosity
ρ	=	density
φ	=	fan flow coefficient, $U/(ND)$

I. Introduction

RECENTLY, Kummer and Dang [1] proposed the so-called *high-lift propulsive airfoil* concept for aircraft applications. The concept involves partially embedding a crossflow fan (CFF) along the trailing edge of the wing. The CFF is basically a two-stage fan with a rectangular cross section that is used extensively in the heating, ventilating, and air-conditioning industry. Figure 1 shows a diagram of the major components of the high-lift propulsive airfoil. The airfoil is a modified Gottingen 570, with the original airfoil truncated and a CFF partially embedded along the trailing edge. By drawing air in over the suction surface, energizing it, and expelling it out of the airfoil trailing edge, the CFF provides many benefits. At low angles of attack, the low-momentum boundary layer is ingested by the fan and reenergized, resulting in increased propulsive efficiencies by filling in the wake region of the airfoil and even creating thrust at sufficiently high rotational speed. At the same time, the fan provides circulation control to the airfoil, greatly increasing the lift coefficient at the cruising condition. For higher angles of attack, the fan has the added ability to maintain flow attachment or to even reattach massively separated flow. As demonstrated through computational fluid dynamics (CFD) analysis [1], such an airfoil is expected to reach significantly higher climb angles (30–40 deg) without experiencing stall and to achieve corresponding lift coefficients of 6–7. Since the completion of this study, it is noted that several flying model airplanes based on this concept have been successfully demonstrated at Syracuse University and Propulsive Wing, LLC.

Although this is not the first design to embed a CFF into an airfoil, it is the first successful attempt to provide a combination of propulsion and circulation control that allows operation at such extreme angles of attack. In 1962, Dornier [2] patented the idea of embedding crossflow fans in the middle of an aircraft wing for "providing lift and/or forward thrust." Harloff and Wilson [3] evaluated a similar concept, and their study included an extensive experimental program to define and improve the performance of a crossflow fan over a wide range of fan rpm and operating conditions. Hancock [4] suggested trailing-edge-embedded CFFs driven by wing-tip and root-mounted turbine engines for distributed propulsion. In 1984, Chawla [5] performed an experimental study on the feasibility of embedding a CFF in the center of a thick airfoil for flow control through boundary-layer blowing, which ducts flow from the airfoil pressure surface and expels it over the suction surface as a jet energized by the fan. Chawla found some success in delaying stall at high angles of attack and attaining increased lift coefficients, but she did not focus on thrust production. A less successful attempt at a combined propulsive/circulation-control (P/CC) airfoil was tried by Lin [6] that incorporated an in-line housing to duct flow from the airfoil leading edge through the fan and onto the suction surface. Although the desire and motivation to use an embedded CFF in a

Presented as Paper 368 at the 45th AIAA Aerospace Sciences Meeting and Exhibit, Reno, NV, 8–11 January 2007; received 20 February 2008; revision received 16 July 2008; accepted for publication 19 September 2008.

*Graduate Student, Department of Mechanical and Aerospace, 149 Link Hall.

†Professor, Department of Mechanical and Aerospace Engineering, 149 Link Hall.

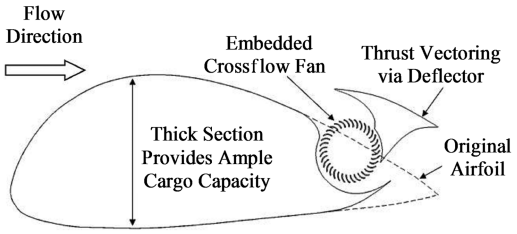

Fig. 1 P/CC airfoil design as suggested by Kummer and Dang [1].

P/CC airfoil is certainly not lacking throughout previous work, the proper fan placement and housing design, it would seem, is lacking.

With the recent advance in CFD methods to handle complex flows, it is now possible to use these computational tools to design airfoils with embedded CFF more effectively. The CFD analysis of a modified Gottingen 570 airfoil with embedded crossflow fan completed by Kummer and Dang [1] shows great promise in many aspects. To validate the CFD findings and determine the effectiveness with which the fan can provide propulsion and circulation control for an airfoil, an experimental program was implemented. A suitable test model was created to measure the surface static pressure and wake total pressure distributions of the prescribed P/CC airfoil at various operating points using the proposed design shown in Fig. 1. In addition, a helium-bubble flow-visualization technique was used to capture images of the flowfield present around the P/CC airfoil with the fan on and off. Finally, the exact geometry of the test model and wind tunnel were simulated in the CFD software package FLUENT to ascertain CFD's ability to accurately predict the influence of the CFF.

II. Experimental Setup

Before this study could be undertaken, much preparatory effort was required to design and construct both the test model and a compatible wind-tunnel facility. Because the results of this study were to be compared directly with those of the previous CFD investigation [1], a geometrically similar model was desired. Accordingly, a 34%-thick Gottingen 570 airfoil section with integrated housing was scaled to fit a commercially available CFF. As described by Holgate and Haines [7], the clearances between the housing walls and fan largely dictate the efficiency of the CFF and are proportional to the fan diameter. Therefore, it was necessary to maintain a sufficiently large fan diameter to avoid excessively precise housing-surface tolerances without significant loss of efficiency. Ultimately, a 5.72-cm-diam fan with 5% wall gaps was chosen, translating to a scaled airfoil of 0.4064 m chord length. Figure 2 shows a scaled representation of the airfoil model with an integrated fan. Note that after truncating the original airfoil and adding the fan housing, the chord line was arbitrarily redefined from the leading edge of the airfoil through the trailing-edge flap. Consequently, the 0 deg angle-of-attack position corresponds to a negative airfoil incidence. Although the housing surfaces were designed and built to be adjustable for future studies on thrust vectoring, the inlet and outlet sizes were fixed at 81 and 68% of the fan diameter for this investigation. To facilitate surface pressure measurement, 27 static pressure taps of 0.84 mm internal diameter were embedded in the airfoil surface, as seen in Fig. 2. Note that the pressure taps extended to only 75% of the chord length and that there were no taps located in the fan housing surfaces, a limitation that will be addressed in Sec. IV. The pressure taps were connected via plastic tubing to a Validyne DP45 low-pressure transducer that interfaced directly with a PC using LabVIEW for data acquisition. The DP45 transducer used in this study had a full-scale range of ± 0.55 in. H_2O and accuracy of 0.5% full scale. This translates to an accuracy of ± 0.68 Pa for all of the pressure data acquired on both the suction and pressure surfaces.

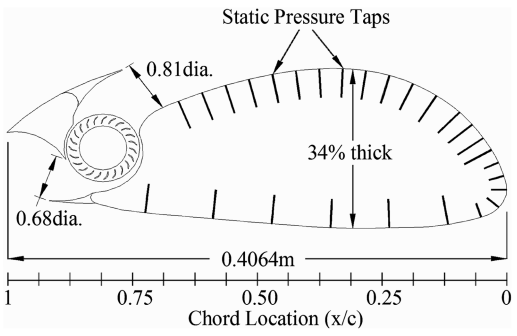

Fig. 2 CFF airfoil model sizing and pressure-tap layout.

For wake total pressure measurements, a pitot rake was placed $1/3c$ downstream of the airfoil model. The rake contained 8 pitot tubes that were sampled with the same pressure transducer and data acquisition system as the surface pressure measurements. In each of the tests, the pitot rake was approximately centered on the fan exhaust jet with a symmetric distribution of tubes above and below the jet. A vernier height gauge was used to precisely position the pitot rake vertically in the tunnel, thereby allowing refined resolution in the wake data via multiple sampling locations.

In addition to the pressure data acquired, flow-visualization images were captured using a helium-bubble-seeding technique to yield a qualitative evaluation of the concept. In this method, neutrally buoyant helium-filled soap bubbles trace the streamlines of the flow and are illuminated with a modulated arc lamp for visualization and image capturing.

Because of the large size of the airfoil model, an existing open-circuit suction wind tunnel with a custom-fitted test section was used to conduct the testing. Note that because a suction tunnel was used, in our definitions of Cp_o and Cp, the freestream total pressure is equal to atmospheric pressure (assuming no loss through the tunnel entrance) and the static pressure in the tunnel, denoted by p_s, therefore equals atmospheric pressure minus the freestream dynamic pressure. The tunnel was driven by a centrifugal blower capable of flow rates up to 6500 ft^3/min and was connected to a test section designed specifically for this study with a cross section that was 1.12 m high by 0.457 m wide, allowing for freestream velocities up to $\sim$6 m/s ($Re_c = 170,000$). To better simulate a 2-D airfoil section, the airfoil model was designed to span the entire width of the tunnel with the CFF also embedded along the full span of the trailing edge. Figure 3 shows the completed airfoil model as installed in the test section. Note that the fan drive system consisted of a direct-drive 1/15 hp dc motor (mounted on the outside of the far side of the tunnel) for which the rotational speed was controlled by a Leeson dc speed controller and measured with both a strobe light and laser tachometer. Because the motor was connected directly to the fan with

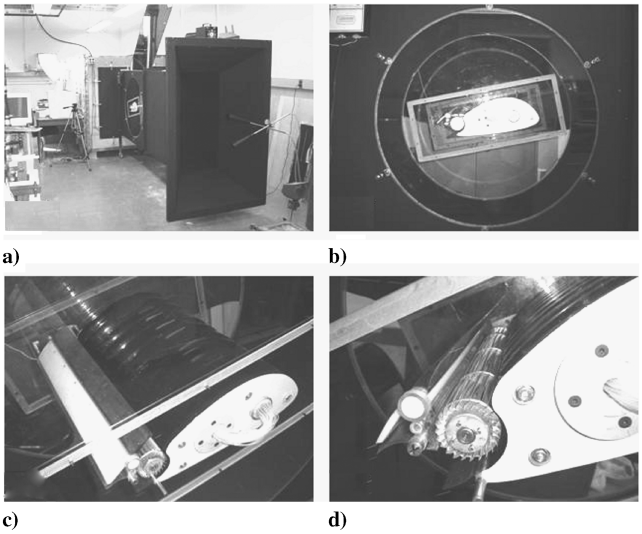

Fig. 3 Photographs of a) completed test section attached to wind-tunnel driver section, b) airfoil mounted in Lexan circles, allowing change in angle of attack, and c–d) completed airfoil model.

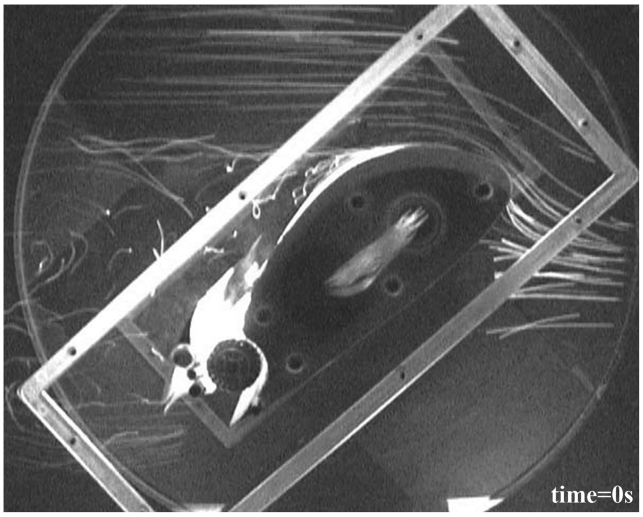

Fig. 4 Fan-off condition, 40 deg angle of attack, and $Re = 85,000$.

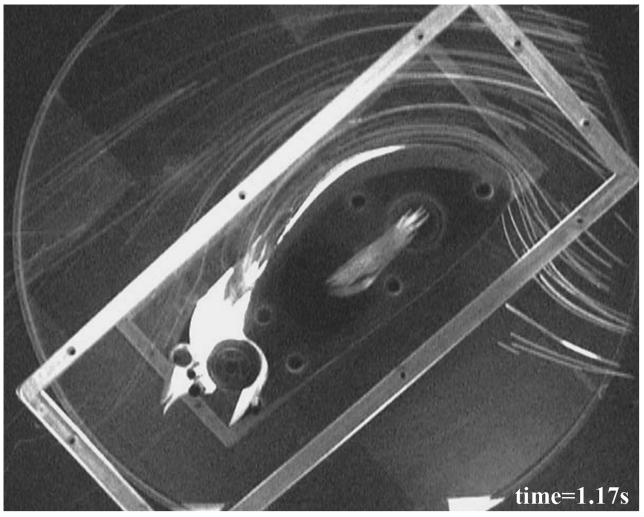

Fig. 5 Fan rpm = 4100 ($\varphi = 0.12$), 40 deg angle of attack, and $Re = 85,000$.

no gearing system, the maximum speed attainable by the fan was limited to 4100 rpm.

III. Experimental Results

As mentioned, two types of testing were conducted in this study: qualitative flow visualization and surface static and wake total pressure measurements. Given the limitations of the flow seeding technique and image-acquisition equipment, quality flow-visualization results were not attainable above a freestream velocity of $\sim$3 m/s ($Re_c = 85,000$). For the pressure measurements, however, tests were conducted at 3.92 and 5.92 m/s ($Re_c = 110,000$ and 170,000, respectively). Two cases were examined using flow visualization: high-angle-of-attack reattachment of massively separated flow and leading-edge stagnation-point movement at low angles of attack with circulation control. For the pressure measurements acquired, a range of cases between 0–45 deg with the fan rpm up to 4000 were tested.

A. Flow Visualization

1. Reattachment/Stall-Free Operation at High Angles of Attack

It is useful to obtain a qualitative viewpoint of the CFF airfoil's flowfield before examining the actual pressure data. To this end, we will turn our attention first to the flow-visualization images acquired during the reattachment of massively separated flow over the CFF airfoil at high angles of attack. Figure 4 shows the airfoil at a 40 deg angle of attack with the fan off and Reynolds number of 85,000. Here, we see that the flow is fully separated from the surface of the airfoil at approximately the quarter-chord location. With the fan off at this extreme angle of attack and early separation, it is expected that the fan housing will have little influence on the flowfield. Consequently, Fig. 4 can be considered to be equivalent to the flowfield of the original airfoil (this is supported by the pressure data presented later for similar high angles of attack). Comparatively, Fig. 5 shows the same configuration with the fan running at 4100 rpm or flow coefficient $\varphi = 0.12$ (note that the flow coefficient defined here is equivalent to the advance ratio commonly used for propellers). The flow is now completely reattached to the surface of the airfoil and smoothly leaving the trailing edge of the fan housing. By ingesting the low-momentum boundary layer along the suction surface and creating a large suction effect, the CFF has eliminated the large separated-flow region on the suction surface that would typically form at such high angles of attack, and it has also greatly reduced the wake size. Note that Fig. 4 depicts the flow directly before the fan is instantaneously brought to 4100 rpm, and Fig. 5 depicts the flow upon reattachment to the airfoil surface 1.17 s later. This indicates that complete reattachment at this severe angle of attack takes on the order of 10 flow times. Other high-angle-of-attack flow-visualization results can be found in [8].

2. Circulation Control at Low Angles of Attack

With a clear demonstration of the CFF's ability to reattach massively separated flow and maintain flow attachment through very high angles of attack, we now wish to examine the effect of the fan at low angles of attack for circulation control. Figure 6 shows the leading-edge stagnation point of the airfoil model at a 10 deg angle of attack. In Fig. 6a, the stagnation point is located at chordwise location $x/c = 0$ for the fan-off case. At the same angle of attack with the fan operating at 1000 rpm ($\varphi = 0.49$), the stagnation point shifts along the pressure surface toward the trailing edge of the airfoil by 1% of the chord length in Fig. 6b. Similarly, at 4100 rpm ($\varphi = 0.12$) in Fig. 6c, the stagnation point moves further back on the pressure surface to 2% of the chord. This demonstrates the CFF's capability of circulation control and shows the opportunity to use the fan for lift augmentation even at low angles of attack. At the same time, it should be recognized that by moving the high-pressure stagnation region from the leading edge to the pressure surface underneath the airfoil, not only has lift increased, but pressure drag has also been reduced (see Sec. III.B). This shows additional promise for the CFF airfoil in applications of thick wing sections that would ordinarily incur very large pressure-drag penalties.

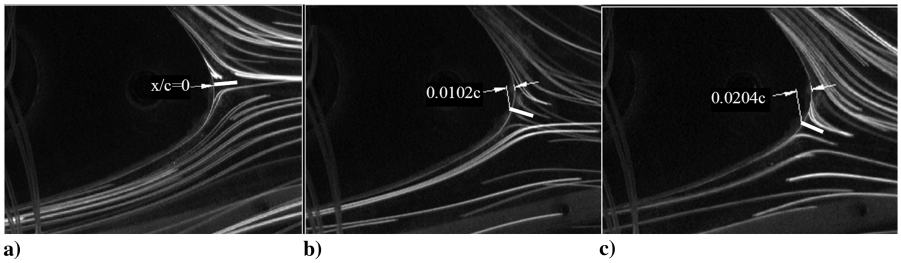

Fig. 6 Leading-edge stagnation point, 10 deg angle of attack, $Re_c = 85,000$, and fan a) off, b) 1000 rpm ($\varphi = 0.49$), and c) 4100 rpm ($\varphi = 0.12$).

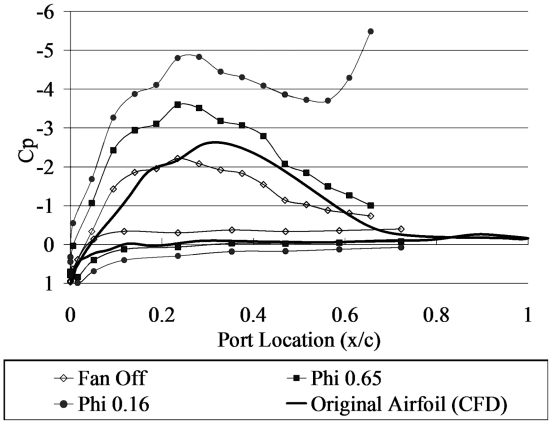

Fig. 7 Pressure coefficient data, 10 deg angle of attack, and $U = 3.92$ m/s.

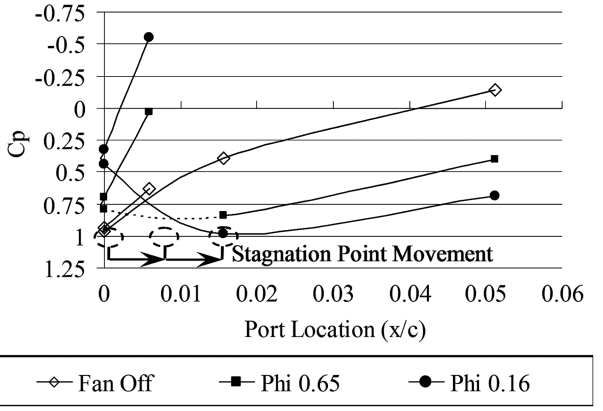

Fig. 8 Leading-edge stagnation-point movement, 10 deg angle of attack, and $U = 3.92$ m/s.

B. Surface Static Pressure

With a qualitative understanding of the CFF's influence on the airfoil, we now turn our attention to the actual static pressure data acquired from the surface of the model for both the circulation-control case at cruising angles of attack as well as the reattachment/stall-free case at high angles of attack. As previously mentioned, the pressure-data tests were conducted with freestream velocities of 3.92 and 5.92 m/s, thereby restricting the stall-free angle of attack to 30 deg for these tests due to the limitation of maximum fan rpm. Note that complete Cp data for all cases studied may be found in [8].

1. *Circulation Control at Cruising Angles of Attack*

When examining the effectiveness of the CFF in providing circulation control to the airfoil, we will focus on the pressure data acquired for the case of a 10 deg angle of attack in which flow separation is mild. Figure 7 depicts the Cp distribution for two fan operating points as well as for the fan-off case and original airfoil for comparison at 10 deg, $U = 3.92$ m/s (note that the original airfoil data was not experimentally available and was instead generated using CFD). By operating the fan even at a high flow coefficient of 0.65 ($N = 1000$ rpm), a significant drop in Cp on the suction surface is observed with a 60% decrease at the suction peak from -2.2 to -3.5. As the flow coefficient decreases to 0.16 ($N = 4000$ rpm), Cp continues to drop significantly on the suction surface, falling 115% lower than the fan-off case near the suction peak. Additionally, the Cp distribution is now completely altered near the fan inlet, due to the large suction effect of the CFF. As shown in the following section, this translates to a large increase in lift over the fan-off case and makes possible the lift coefficients that are normally attainable only at high angles of attack.

Continuing to Fig. 8, the stagnation-point movement observed in the flow-visualization experiments is now portrayed in the acquired Cp data. Here, as before, the leading-edge stagnation point is found to lie at approximately $x/c = 0$ for the fan-off case, as given by $Cp = 1$ at that point. Corroborating the results from Fig. 6, the stagnation point shifts rearward on the pressure surface to $\sim$0.8% of the chord length as the fan is turned on to $\varphi = 0.65$. As expected, the stagnation point continues to move downstream ($\sim 1.7\%c$) as the flow coefficient decreases to 0.16. By moving the stagnation region, the Cp value at the leading edge of the airfoil has dropped to 0.4 for the $\varphi = 0.16$ case, illustrating the decrease in pressure at that point and the potential for lower pressure drag. Although the stagnation-point shifts displayed in the Cp data are not as large as those from the flow visualization, it must be remembered that the flow coefficients for these tests are not matched exactly.

2. *Reattachment/Stall-Free Operation at High Angles of Attack*

Now considering the CFF's ability to reattach massively separated flow at high angles of attack, Fig. 9 shows the Cp distributions acquired at a 30 deg angle of attack with $U = 3.92$ m/s. At this large angle of attack, the airfoil is stalled with the fan off. Note that the original airfoil CFD data nearly matches that of the fan-off CFF airfoil test data, indicating that at this high angle of attack, the housing has little influence on the flow when the fan is off. With the fan operating at $\varphi = 0.22$ ($N = 3000$ rpm), however, the flow reattaches to the surface of the airfoil with a 230% decrease in pressure at the suction peak and a Cp distribution thereafter, corresponding to fully attached flow. Decreasing the flow coefficient further results in an additional drop in suction surface pressure, indicating that the fan is capable of yielding further circulation control even at high angles of attack once fully attached flow has been achieved. Recognizing that the area between the Cp curves of the suction and pressure surfaces represents the lift force per unit span generated by the airfoil, this substantial decrease in suction surface pressure translates to a large increase in C_l for the CFF airfoil.

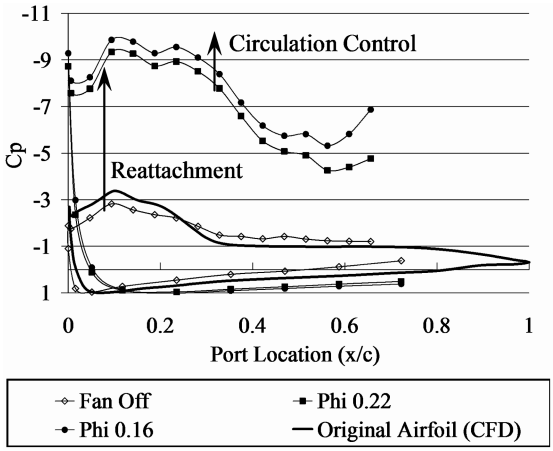

Fig. 9 Pressure coefficient, 30 deg angle of attack, and $U = 3.92$ m/s.

3. *Lift Coefficient*

Integrating the static pressure along the surface of the airfoil, we are able to approximate the lift coefficient of the section containing the pressure ports. Admittedly, this estimate of C_l is not exact in that it does not account for the lift contribution of the fan, fan housing, and airfoil trailing edge (refer to CFD results in Sec. IV), nor does it consider the jet vertical momentum flux expelled from the fan. Figure 10 shows the lift curve for all angles of attack tested at $U = 3.92$ m/s. From here, we see that lift coefficients upward of 7 are achievable for stall-free operation at a 35 deg angle of attack with the CFF operating at $\varphi = 0.1$, highlighting the reattachment ability of the CFF airfoil. Equally interesting, however, is the ability to obtain $C_l \sim 3$–4 at cruising angles of attack by using the fan to alter circulation (around 5–10 deg angles of attack). In Fig. 10, the stall point for each fan flow coefficient is clearly visible, with a linear

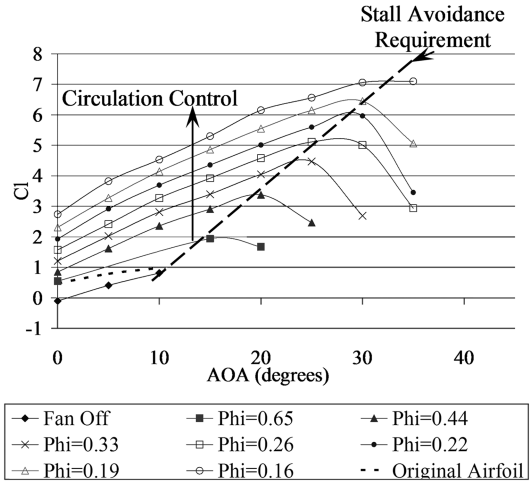

Fig. 10 Calculated lift coefficients.

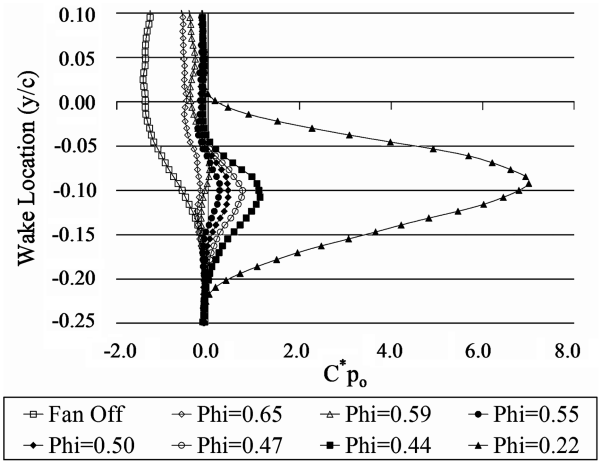

Fig. 11 Wake/jet total pressure, 15 deg angle of attack, and $U = 3.92$ m/s.

trend dictating the fan requirement for stall avoidance at each angle of attack. All operating points to the left of the stall-avoidance line represent added circulation control to the airfoil, and all points to the right represent stall. As indicated previously, lower fan flow coefficients (or higher fan rpm) are expected to produce similar results, with increased circulation control and further stall delay at higher angles of attack. If we examine the lift-curve slope of each flow coefficient curve in Fig. 10, we find that it closely matches simple potential flow theory for elliptical shapes:

$$\frac{dC_l}{d\alpha} = 2\pi\left(1 + \frac{t}{c}\right)$$

Furthermore, it is interesting to note that the C_l intercept of each flow coefficient curve found here closely follows the function $0.45(\varphi^{-1})$. These two details allow us to define the lift coefficient in terms of α and φ: in this case,

$$C_l = 2\pi(1 + t/c)\alpha + 0.45(\varphi^{-1})$$

Note that the lift curves of Fig. 10 are plotted in terms of fan flow coefficient; therefore, this family of lift curves is applicable to other freestream velocities if the data acquired is shown to be Reynolds number independent for geometrically similar cases. Section III.D will examine and compare the acquired data using dimensional analysis to illustrate its Reynolds number independence.

C. Wake Total Pressure

In addition to the surface pressure data acquired in this study, a limited number of detailed wake total pressure measurements were obtained to ascertain the full effect of the CFF on the airfoil's wake/jet region. The wake/jet total pressure was measured in detail for only one angle of attack, 15 deg, whereas other angles of attack were examined in lower resolution. Accordingly, only the data from the 15 deg case is meaningful on its own and will be considered here, and the remainder of the wake/jet total pressure measurements can be found in [8].

Figure 11 yields the detailed total pressure measurements in the wake/jet region for the 15 deg angle-of-attack case with $U = 3.92$ m/s, given here in terms of $C^* p_o$. Because the pitot rake is always aligned with the freestream flow direction, the pressure measurement is actually the total pressure minus the dynamic pressure associated with the local vertical-velocity component. Given that the vertical component of the velocity may become significant at high angles of attack, we make the distinction of the corrected total pressure coefficient, denoted as $C^* p_o$ (for the 15 deg case examined here, however, CFD results indicate the dynamic pressure due to the vertical-velocity component of the jet accounts for only 3% of the total pressure).

The main interest here was to analyze the effect of the CFF on the wake of the airfoil, especially in the range of reattachment. From Fig. 10, we find that reattachment is expected to occur for fan operation between $\varphi = 0.65$ ($N = 1000$ rpm) and $\varphi = 0.44$ ($N = 1500$ rpm) for the current case. Using this knowledge, total pressure data was sampled at 100 rpm increments within this range of fan operation to more closely study the transition from separated to reattached flow. As would be expected, with the fan turned off we find a large wake region downstream of the airfoil, as indicated by the negative $C^* p_o$ values in Fig. 11. Operating the fan at $\varphi = 0.65$ results in a large decrease in the wake size; however, there is still a region of total pressure deficit present. Similarly, for $\varphi = 0.59$, the wake decreases slightly more, with even a small jet of positive total pressure appearing around the wake-height location of $y/c = -0.075$. This wake-filling aspect of the CFF airfoil translates to increased propulsive efficiency. Recall that Kummer and Dang [1] have shown through their CFD work that propulsive efficiency greater than 1 can be achieved with the current concept.

Also rather interesting is the sudden and obvious change in wake structure when φ is decreased now to 0.55. For this and all subsequent flow coefficients, the total pressure deficit of the wake region virtually disappears and remains constant at $C^* p_o \sim 0$ or freestream total pressure, with the significant appearance of a high-total-pressure jet issued from the fan, which continuously increases in strength and size as the fan rotational speed is increased. This important piece of information clearly indicates that in the case of high-angle-of-attack operation in which separated flow exists, the CFF has a distinct point of operation that is necessary for complete reattachment and wake reduction. Further increasing the fan's rotational speed beyond this point results in net thrust production and, ultimately, augmented circulation.

D. Dimensional Analysis

In this section, we use dimensional analysis to organize our test data so that the results can be scaled appropriately based on desired flight conditions. Figure 12 plots the comparison between the two freestream velocities tested at a fixed 10 deg angle of attack and $\varphi \sim 0.25$. Here, we find excellent agreement between both sets of data for a fixed flow coefficient, indicating that the assumption of Reynolds number independence holds for this case. Moving to Fig. 13, similar results are found from the comparison at a 30 deg angle of attack and $\varphi \sim 0.25$. Although the data agreement at this high angle of attack is slightly lessened from that of 10 deg, this is explained by the close proximity to the stall condition at which we are operating (again, limited by the fan's maximum rpm in our test). We note that the Reynolds number based on the chord of the airfoil studied here is relatively low (less than 200,000), and hence we expect the concept to also hold at higher Reynolds numbers. This is very encouraging in that it allows the accurate construction and use of

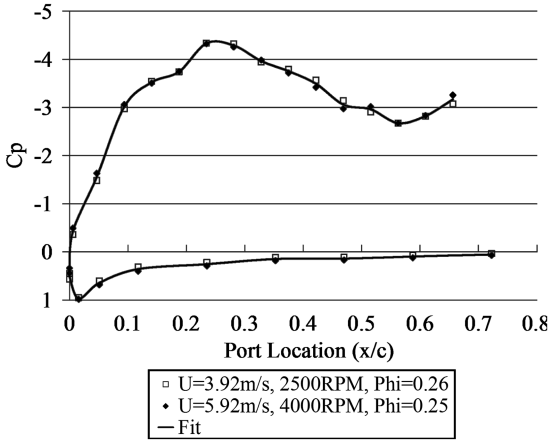

Fig. 12 Fan law comparison at a 10 deg angle of attack.

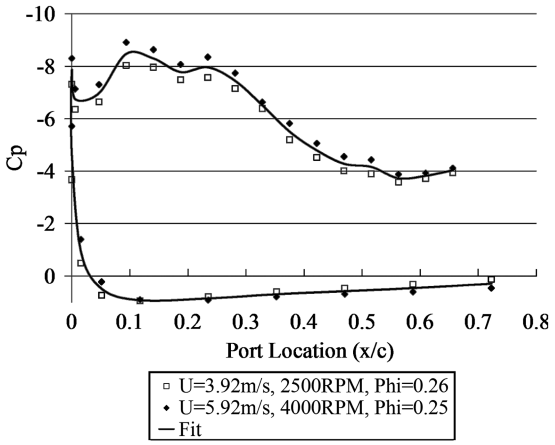

Fig. 13 Fan law comparison at a 30 deg angle of attack.

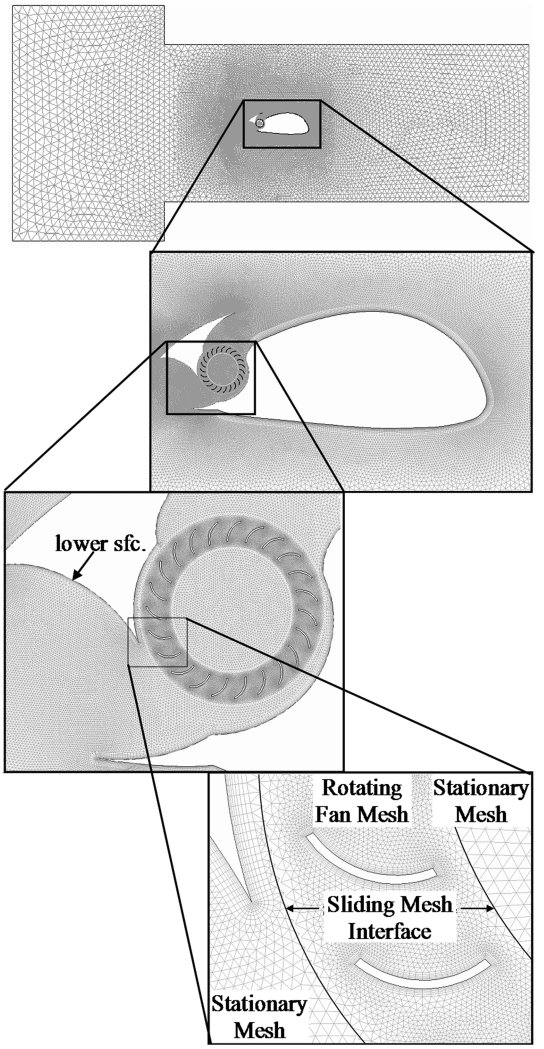

Fig. 14 CFD comparison grid at a 0 deg angle of attack.

the family of lift curves displayed in Fig. 10, which yields the fan operating point requirements for desired circulation control and stall-free operation based solely on the selected angle of attack.

IV. CFD Comparison

A. CFD Setup

In addition to the experimental data acquired in this study, select cases were simulated using the CFD software package FLUENT to examine CFD's ability to accurately predict the flowfield around the CFF airfoil and the influence of the CFF in terms of reattachment and circulation control. Cases were setup at 0, 15, and 30 deg angles of attack for the geometrical model used in the experiment with the flow velocity of all cases set at 3.92 m/s. The original AutoCAD drawings used as templates for construction of the test model with the proper airfoil sizing and inlet and outlet dimensions and angles of the fan housing were exported to the grid-generation software Gambit to produce the computational model. Although the test model sizing was reproduced to within ± 0.064 cm of the original design, the skin contained spanwise variations due to distortion between ribs (see Fig. 3c) that was not captured in the CFD model's two-dimensional geometry. Additionally, the off-the-shelf fan lacked geometrical data for use in constructing the computational fan model. Although the blade size, shape, and angle were measured for approximation in the CFD model, the fan was composed of crude sheet-metal blades bent roughly in the shape of circular arcs with loose geometric tolerances, making exact replication extremely difficult. The low-tech nature of the fan with its square-cornered leading- and trailing-edge blades (depicted in Fig. 14) results in inherently low fan performance, with frequent flow separation occurring on the blades. Kummer [9] carried out a CFD study to evaluate the effects of blade geometry on fan performance and showed that these square-end blades performed very poorly compared with rounded-end blades. These factors make accurate modeling of the flow through the fan difficult in our CFD simulations and may account for some of the variation between the CFD and experimental results.

To compare appropriately with the test data, all three grids duplicated the geometry of the wind-tunnel height and its relation to the airfoil model because tunnel-wall effects become significant at high angles of attack. Figure 14 shows the grid for the 0 deg case. The 15 and 30 deg cases were identical, with only the airfoil angle of attack changing. A hybrid grid was used, composed of quad mesh around the airfoil and fan geometries and triangular mesh elsewhere. Each grid was composed of approximately 166,000 cells and used a sliding-mesh interface between the rotating fan region and the main grid region, as seen in Fig. 14. The grid density around the fan and the airfoil was based on the work reported by Kummer [9]. A uniform-velocity inlet boundary condition was specified at the wind-tunnel entrance and a pressure outlet was implemented at the exit of the plenum. Second-order upwind discretization was used with FLUENT running in double-precision mode. Although the Reynolds number based on the airfoil chord was only 110,000, and hence the flow was likely to be in the transitional range, a fully turbulent flow was assumed. The standard k-ε model with enhanced wall treatment was selected in these simulations, with y^+ values below 3 on the fan blades, below 2 on the airfoil main surface, and below 4 on the fan housing surfaces. With respect to lift prediction, the flow around the airfoil is expected to behave like an inviscid flow when the fan is operated at sufficiently high rpm so that the flow is fully attached to the airfoil and hence the viscous effect is of second order, minimizing the error due to CFD modeling.

It is important to note that unsteady simulation of the complete CFF airfoil with a rotating fan is necessary to adequately model the effects of the fan. Especially in the case of high-angle-of-attack operation, the exhaust jet of the fan is responsible for entraining the low-momentum flow above the fan housing and, in turn, reattaching and maintaining the flow on the airfoil's suction surface. Because the exhaust jet is highly nonuniform, it is imperative that it is properly captured to accurately reproduce its influence on the airfoil. In this light, use of an actuator disk approximation would require prior knowledge and specification of the exhaust profile. Also, use of the multiple reference frame steady-flow model in FLUENT [10] fails to capture the dynamic lift effect on the CFF blades and subsequently fails to adequately reproduce the proper fan-performance characteristics (and hence the exhaust jet). Using the guidelines set forth in [9], the time step for the unsteady calculation was found by dividing the blade passage period by 20 to provide sufficient resolution of the fan's rotation. The lift and drag coefficients were monitored during the calculation to determine when they ceased significant oscillation, indicating convergence. In all cases, the residuals for every parameter decreased to at least 10^{-7} by the time the lift and drag had leveled out. Once the unsteady solution had converged, the simulation was run for an additional 10 fan revolutions while the time-averaged data was computed. All cases were run on 4 nodes of a 30-node Beowulf cluster equipped with dual-core AMD Opteron CPUs. Computational time was on the order of 4–5 days.

B. Comparison of CFD Results with Test Data

Because we are mainly interested in the ability of CFD to predict the effect of the CFF on the pressure distribution of the airfoil, we will look only at those cases of fully attached flow in which the fan is turned on. To begin, we will examine the CFD results for the surface pressure coefficient at a 15 deg angle of attack. Figure 15 shows the CFD comparison at $\varphi = 0.22$ ($N = 3000$ rpm). At this operating point, the flow is fully attached and CFD does an excellent job of accurately predicting not only the pressure distribution on both surfaces, but also the magnitude; in this case, CFD only slightly overpredicts the airfoil peak suction and slightly underpredicts the suction pressure just ahead of the fan inlet. For the 30 deg angle-of-attack case, Fig. 16 again shows very similar trends between the CFD results and our experimental data. Further comparisons between the CFD and experimental surface pressure data are given in [8] for the select angles of attack and fan operating points simulated. In all comparisons, the agreement is similar to those shown here, with CFD slightly overpredicting the peak suction on the airfoil and slightly underpredicting the suction at the fan inlet. Recall that the spanwise distortion in the physical experimental model was not captured in the two-dimensional CFD simulations and may account for the difference in peak suction pressure on the airfoil surface. From these results, it is apparent that accurate prediction of both the flow-attachment and circulation-control aspects of the CFF airfoil with this configuration and CFF setup are possible using CFD, indicating the potential to use CFD as an adequate design tool for future work.

As noted in the C_l discussion in Sec. III.B, test data is not available on the fan housing, and we rely on CFD to quantify the contribution of lift from the fan and fan housing. From Table 1 we see that in the CFD cases studied here, the fan contributes negatively to the overall lift coefficient, whereas the fan housing and trailing-edge airfoil surfaces contribute positively. For a 15 deg angle of attack, a negligible change in overall C_l is seen, with the positive contribution from the fan housing canceling the negative contribution of the fan itself. By 30 deg, the positive contribution from the fan housing significantly outweighs the negative contribution from the fan; however, the net change in C_l is still small, given the large lift

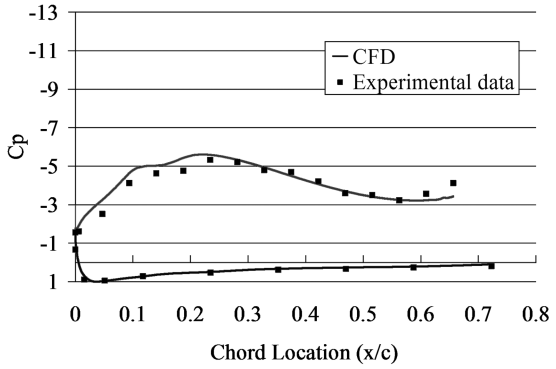

Fig. 15 CFD comparison for a 15 deg angle of attack and $\varphi = 0.22$.

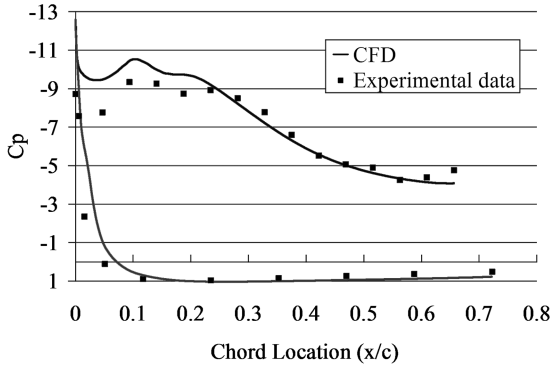

Fig. 16 CFD comparison for a 30 deg angle of attack and $\varphi = 0.16$.

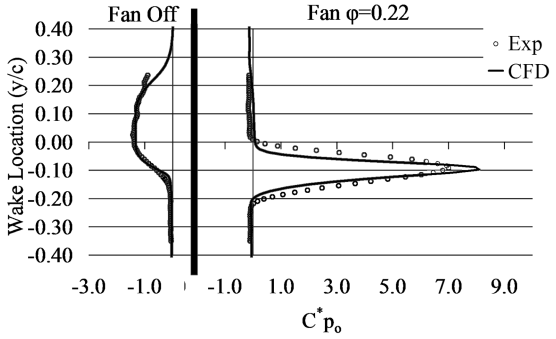

Fig. 17 Wake/jet region for a 15 deg angle of attack.

generation of the forward airfoil section. In each of the cases studied, the lower surface of the fan housing, labeled in Fig. 14, contributes nearly all of the net positive lifting force on the housing. This is due to the curvature of the housing surface and turning of the high-pressure jet exhausting from the fan along this surface. The CFD results show that the contributions of the fan and housing surfaces cannot be neglected in the overall design of the CFF airfoil. Because the fan housing's lift production is significant, the possibility of using the housing surfaces for directional control by changing surface position to alter the lift force present is also shown to be viable despite its limited moment arm.

Looking now to the comparison of CFD with our experimental wake total pressure data, we will examine the detailed data acquired at a 15 deg angle of attack and $\varphi = 0.22$, seen previously in Fig. 11.

Table 1 Fan and housing lift-coefficient contributions from CFD

	Forward airfoil C_l	Housing C_l	Fan C_l	Net system C_l	System C_l change
15 deg, $\varphi = 0.22$	4.4	0.81	−0.92	4.29	−2.50%
30 deg, $\varphi = 0.16$	7	0.71	−0.25	7.46	6.60%

Table 2 Corresponding fan Reynolds numbers

RPM	1000	1500	2000	2500	3000	3500	4000
Re_f	1211	1816	2422	3027	3632	4238	4843

Note that additional coarse experimental data comparisons with CFD wake results are included in [8], with results similar to those witnessed here. Figure 17 depicts the wake/jet region present with the airfoil at a 15 deg angle of attack. In the left frame, we see that the wake with the fan turned off reaches a C^*p_o value of approximately -1.5. Note that negative values of C^*p_o represent the total pressure loss, $C^*p_o \sim 0$ indicates the freestream condition (recall that C^*p_o is the total pressure *minus* the dynamic pressure due to the vertical-velocity component), and positive C^*p_o represents an increase in total pressure due to the fan. For the fan-off case, the wake-region total pressure deficit is predicted quite well by CFD in the range of experimental data available. In the right frame of Fig. 17, we see that operating the fan at $\varphi = 0.22$ results in a complete filling of the wake region and the production of a jet with $C^*p_o = 7$–8 (and hence the presence of thrust production). In this case, we see that the CFD results yield a slightly stronger jet with higher maximum total pressure rise and less spreading than what was actually measured in the experiment. Here, it is important to note that the prediction of the jet is directly dependent on the modeling of the fan itself, along with the ability of CFD to accurately predict the flow through the fan. From this data it becomes evident that the fan can indeed be used as a propulsion source, either in whole or as a supplement to a hybrid propulsion system. Also, because the fan is capable of filling the wake region of the airfoil, the potential for drag reduction and increased propulsive efficiency becomes more tangible, even in the case of thick-wing or high-angle-of-attack operation.

Note that in all of the experimental cases studied here, the Reynolds number based on the fan, Re_f, is quite low. Table 2 shows the corresponding fan Reynolds numbers. It has been shown in various studies that fan performance experiences a significant drop when operating below $Re_f \sim 7000$–$10,000$, depending on the vortex wall shape (see Lazzarotto et al. [11]). In these experiments, the highest fan Reynolds number was on the order of 5000, showing that we are operating in the range of Re_f in which the fan's performance is poor. This being said, with the good agreement we have seen both with CFD and fan laws in this study, it can be expected that the correlation will only become better as Re_f increases into the regime in which performance is independent of Re_f. In addition, as Re_f increases, performance is expected to increase, indicating that the respective rpm requirements (and hence power requirements) seen in this study will continue to decrease. Given the low Reynolds numbers at which the tests were conducted, the flow in the CFF is expected to be transitional, whereas our CFD simulations assume a fully turbulent flow. This may also account for some of the variation between our CFD and experimental wake data.

V. Conclusions

An extensive experimental study of the viability of embedding a crossflow fan (CFF) in the trailing edge of a thick airfoil for simultaneous propulsion and circulation control was undertaken. Flow visualization yields clear proof that the CFF is capable of not only reattaching massively separated flow at high angles of attack and maintaining flow attachment, but also that the fan can provide significant circulation control to the airfoil for lift enhancement at cruising angles of attack. Surface pressure data indicates the ability to reattach separated flow by a significant decrease in pressure on the suction surface upon reaching the reattachment fan speed range, also showing the capability to attain lift coefficients upward of 6–7 while operating stall-free to 30 and 40 deg angles of attack. Further increasing the fan's rotational speed beyond the point of reattachment offers even higher lift coefficients as the circulation-control aspect of the fan is realized. In this case, pressure data indicates lift coefficients of 3–4 are achievable even at cruising angles of attack. Additionally, an examination of the wake/jet region of the CFF airfoil indicates its ability to completely fill in the wake region, thereby reducing drag and increasing propulsive efficiency. At a sufficiently high fan rotational speed, the CFF airfoil can even create excess thrust, showing its potential as a propulsion source.

Computational fluid dynamics (CFD) comparison with the experimental work conducted in this study has yielded good agreement, especially given the deficient fan-performance range examined. This is promising because it illustrates the ability to use CFD to accurately model the CFF airfoil and effectively use it as a design and analysis tool in future CFF airfoil studies. It must be remembered, however, that it is important to properly model the CFF airfoil in its entirety with an unsteady rotating fan to properly predict the influence of the fan on the flowfield of the airfoil. Even small discrepancies in modeling fan geometry may impact the calculation of fan performance, thereby altering the effect that the CFF has on the airfoil and improperly predicting flow entrainment on the suction surface behind the fan, the wake/jet structure, and surface pressure distribution of the CFF airfoil.

Acknowledgments

R. K. Dygert was funded as a NSF GK-12 Graduate Teaching Fellow. The authors would like to thank Nichole Nadermann, Justin Ruball, and Khang Nguyen for their assistance in pressure-data acquisition and reduction for many of the tests conducted in this study. Special consideration is extended to Joseph Kummer for his assistance in conducting the computational fluid dynamics calculations and for his inputs during this study.

References

[1] Kummer, J., and Dang, T., "High-Lift Propulsive Airfoil with Integrated Crossflow Fan," *Journal of Aircraft*, Vol. 43, No. 4, Aug. 2006, pp. 1059–1068.

[2] Dornier, P., "Multiple Drive for Aircraft Having Wings Provided with Transverse Flow Blowers," U.S. Patent 3,065,928, filed 27 Nov. 1962.

[3] Harloff, G. J., and Wilson, D. R., "Cross Flow Propulsion Fan Experimental Development and Finite Element Modeling," AIAA 18th Aerospace Sciences Meeting, AIAA Paper 80-0385, Pasadena, CA, 1980.

[4] Hancock, J. P., "Test of a High Efficiency Transverse Fan," 16th AIAA/SAE/ASME Joint Propulsion Conference, AIAA Paper 80-1243, Hartford, CT, 1980.

[5] Chawla, K., "Optimization of Cross Flow Fan Housing for Airplane Wing Installation," M.S. Thesis, Univ. of Texas at Arlington, Arlington, TX, 1984.

[6] Lin, C.-H., "A Wind Tunnel Investigation of the External Aerodynamics of an Airfoil with an Internal Cross Flow Fan," M.S. Thesis, Univ. of Texas at Arlington, Arlington, TX, 1986.

[7] Holgate, M. J., and Haines, P., "Scaling of Cross Flow Fans: An Experimental Comparison," *Journal of Mechanical Engineering Science*, Vol. 20, No. 4, 1977, pp. 27–31.

[8] Dygert, R., "Experimental Validation of Embedded Crossflow Fan Propulsive/Circulation Control Airfoil," M.S. Thesis, Dept. of Mechanical and Aerospace Engineering, Syracuse Univ., Syracuse, NY, 2005.

[9] Kummer, J. D., "Simulation of the Crossflow Fan and Application to a Propulsive Airfoil Concept," Ph.D. Thesis, Dept. of Mechanical and Aerospace Engineering, Syracuse Univ., Syracuse, NY, 2006.

[10] FLUENT, Software Package, Ver. 6.3, Fluent, Inc., Lebanon, NH, 2006.

[11] Lazzarotto, L., Lazzaretto, A., and Martegani, A. D., "On Crossflow Fan Similarity: Effects of Casing Shape," *Journal of Fluids Engineering*, Vol. 123, Sept. 2001, pp. 523–531. doi:10.1115/1.1379033

F. Liu
Associate Editor